We are IntechOpen,
the world's leading publisher of
Open Access books
Built by scientists, for scientists

6,900
Open access books available

185,000
International authors and editors

200M
Downloads

154
Countries delivered to

Our authors are among the

TOP 1%
most cited scientists

12.2%
Contributors from top 500 universities

CLARIVATE ANALYTICS

BOOK CITATION INDEX

INDEXED

WEB OF SCIENCE™

Selection of our books indexed in the Book Citation Index
in Web of Science™ Core Collection (BKCI)

Interested in publishing with us?
Contact book.department@intechopen.com

Numbers displayed above are based on latest data collected.
For more information visit www.intechopen.com

Chapter

Photoacoustic Spectroscopy of Gaseous and Condensed Matter

Surya Narayan Thakur

Abstract

A brief historical account of photoacoustic (PA) effect is followed by a simple mathematical model for the generation of PA signals due to nonradiative transitions in atoms and molecules. Some experimental setups, with microphone and piezo-electric transducers, are described for recording PA spectra of gaseous, solid, and liquid samples. Applications of PA spectroscopy in the investigation of harmful chemicals are presented with illustrative examples. The principle of photoacoustic imaging (PAI) is discussed along with examples of molecular imaging of biological tissue and internal organs in small animals.

Keywords: photoacoustic effect, nonradiative decay, microphone, piezoelectric transducer, photoacoustic cell, aerosols, explosives, actinides, hyperspectral imaging, molecular imaging, photoacoustic microscopy (PAM), photoacoustic tomography (PAT)

1. Introduction

Photoacoustic imaging (PAI) is a novel method of obtaining spectral images of chemical constituents of a sample or a scene, to gain valuable insight into its structure and dynamics. It is based on the technique of photoacoustic spectroscopy (PAS) and covers the entire spectral range from the ultraviolet to the infrared. When light is incident on a sample, photons can be either absorbed, transmitted, or reflected, and the PAS technology focuses on the amount of absorption and its subsequent release as heat. PAS is an extremely sensitive detection technique as it can detect molecular concentrations below the parts per billion (ppb) level. This technique emerged from the discovery of the photoacoustic effect by Graham Bell in 1880 during his attempt to transmit sound over a beam of sunlight [1]. However, it remained dormant for almost a century until the advent of tunable lasers in the 1970s and was successfully used by Kreuzer and Patel for the trace detection of atmospheric pollutants [2].

1.1 Photophone and the spectrophone

Bell succeeded in wireless audio communication about two decades before the radio transmission. He used the newly discovered selenium cell in the receiver in view of selenium's property to react to modulated intensity of sunlight incident on it, as the resistance of selenium crystal depends on the incident light. A flexible mirror was attached at the speaking end of the photophone that created slight

deviation of the beam of light reaching the receiver end. This led to variation of intensity at the selenium receiver, which acted like an optical version of the electric coil in the telephone receiver, converting the intensity modulated light back into sound. Bell performed many experiments and observed that sound waves were also produced directly from a solid sample when exposed to a periodically modulated beam of sunlight as illustrated in **Figure 1**. A hearing tube, whose other end was tightly attached to the open end of a transparent glass test tube with sample placed at its closed end, could be used as a photophone. When a beam of sunlight focused on the sample was rapidly interrupted with a rotating slotted wheel at an audible frequency, the intensity of sound in the hearing tube was dependent on the type of material. The loudest sound was heard when the sample was carbon black, leading to the conclusion that photoacoustic effect was caused by the absorbed light energy which subsequently heats the sample.

During Bell's visit to England in 1880, John Tyndall performed the photoacoustic experiment in gases, and although the photoacoustic effect was confirmed, Tyndall was of the view that it was caused mainly by the radiant heat [3]. Bell was driven by rare intellectual curiosity to learn, and it led him to invent the spectrophone to find out the wavelengths that were more efficient for the radiant heat [4]. For this purpose he converted a prism spectroscope into a spectrophone by replacing the eyepiece of the telescope with a hearing tube in which a thin wire mesh coated with lampblack was fitted in the position of the cross wires (see **Figure 2**). When the incident sunlight was interrupted by a mechanical chopper, the hearing tube pro-duced sound whose frequency was equal to the periodic intermittence of light. The loudness of sound, however, varied in accordance with the intensity of the solar spectrum, being maximum in the green-yellow region and decreasing at both the red and violet ends, and observations were made by fixing the position of the telescope in different spectral regions of the solar spectrum. These observations confirmed the fact that the photoacoustic effect is due to optical absorption, since lampblack totally absorbs light at each wavelength. On the basis of his observations, Bell made the prophetic statement about the great importance of photoacoustic spectroscopy in the infrared.

The interaction between light and matter giving rise to photoacoustic effect has three distinct features. (1) The absorbed energy of optical radiation is converted into heat. (2) At the site of optical absorption, there is a temporal rise and fall of
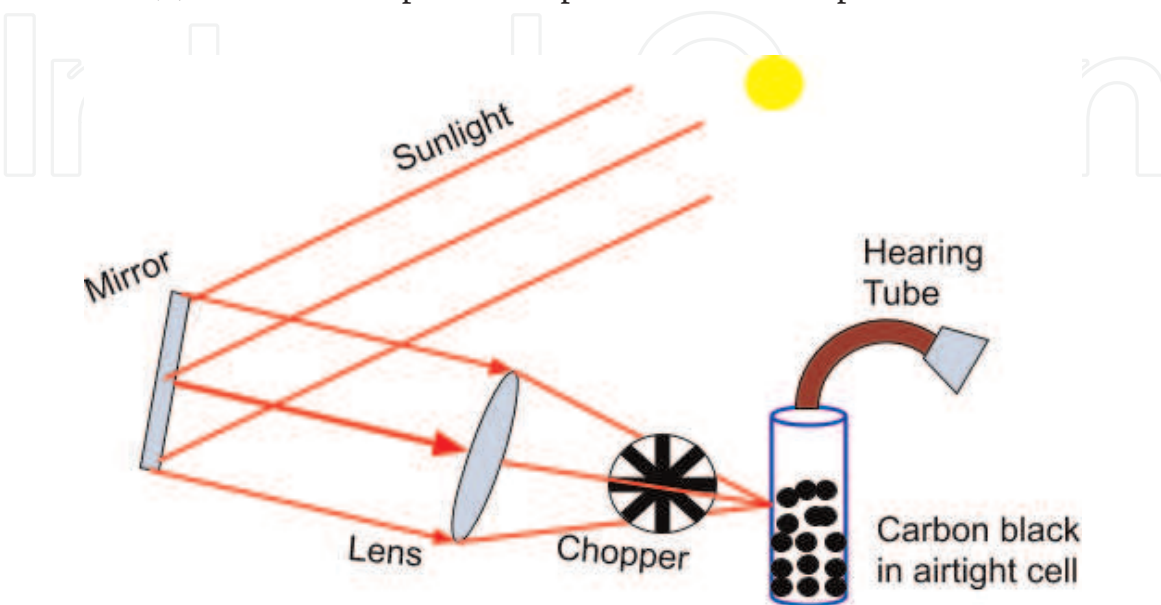
Figure 1.
Illustration of photoacoustic effect with periodically chopped light incident on carbon black sample cell fitted with a hearing tube.
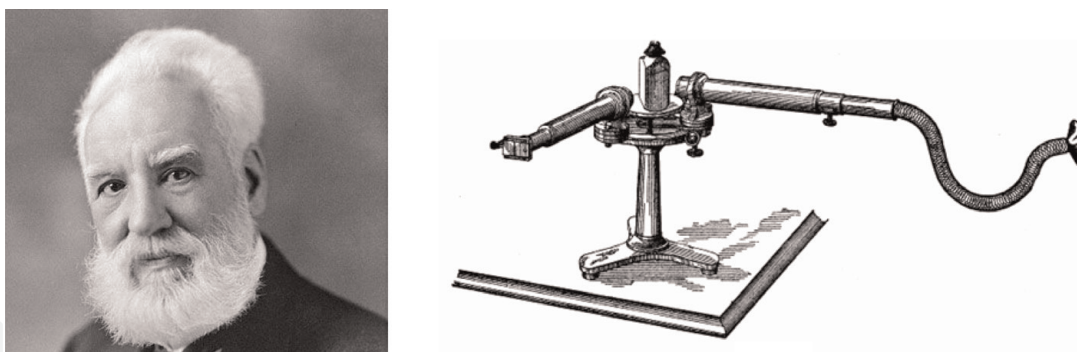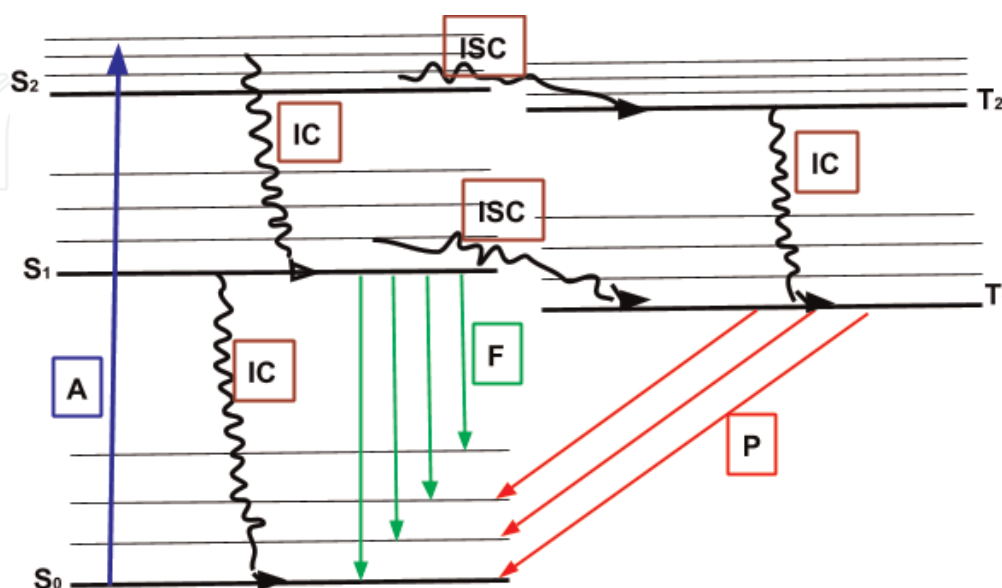
Figure 2.
Alexander Graham Bell and his spectrophone.

temperature. (3) The expansion and contraction following these temperature changes lead to periodic pressure variation to generate sound.

2. Nonradiative transitions and PA signal generation

The heat generation following optical absorption is caused by internal motions in molecules or those of the matrix in which atoms are imbedded in condensed matter. In the quantum mechanical description, an excited molecular state reached by the optical absorption has two channels of relaxation. The radiative decay leads to optical emission, whereas the nonradiative decay causes heating. Thus a molecule, optically excited to a vibronic or a rovibrational state, loses a part of its excitation energy as heat leading to the photoacoustic signal. The photoacoustic spectrum is similar to the absorption spectrum, but its intensity at the exciting wavelength is proportional to the product of the absorption coefficient and the probability of nonradiative decay of the excited state.

Figure 3 shows the energy level diagram, in the Born-Oppenheimer approximation, of a typical organic molecule with an even number of electrons where total internal energy $E = E_e + E_v + E_r$. The rotational energy levels are not shown for the sake of simplicity, and only one of the 3N-6 (or 3N-5) normal modes for a nonlinear

Figure 3.
Typical energy level diagram of an organic molecule where radiative processes A, F, and P stand for absorption, fluorescence, and phosphorescence, respectively. The nonradiative processes IC and ISC refer to internal conversion (IC) and intersystem crossing (ISC), respectively.

(or linear) molecule with N atoms is depicted for the various electronic states. In a large molecule like benzene, nonradiative decay from excited states occurs even in the vapor phase. Michael Kasha pioneered the investigations on nonradiative transitions, and it was found that radiative emission occurs only from the lowest excited state of any multiplicity [5]. The concept of triplet state (T) was first given by Lewis and Kasha [6] to explain the origin of phosphorescence emission in organic or inorganic molecules. Internal conversion (IC) refers to the nonradiative transfer of a molecule from an excited vibronic state to a lower vibronic state of the same multiplicity, whereas intersystem crossing (ISC) corresponds to nonradiative transition between a singlet (S) and a triplet (T) state. Lewis and Kasha formulated a fundamental law concerning fluorescence and phosphorescence through intersystem crossing [6].

2.1 Generation of photoacoustic signal in gases

The rate of radiative transition r_{ij} between two states of a molecule E_i and $E_j(<E_i)$ in terms of Einstein coefficient of stimulated (B_{ij}) and spontaneous (A_{ij}) emission is of the form

$$r_{ij} = \rho(\nu)B_{ij} + A_{ij} \tag{1}$$

where $B_{ij} = B_{ji}$ and $\rho(\nu)$ is the spectral energy density at the frequency ν of the transition. For a two-level system of energy E_0 and E_1 shown in **Figure 4**, we have $B_{01} = B_{10}$ and $A_{01} = 0$, since spontaneous emission from a state of lower energy to one of higher energies does not occur. If c_{ij} represents the probability of a nonradiative (collisional) transition between a pair of states, we assume the collisional excitation from E_0 to E_1 to be very small so that $c_{01} = 0$.

Suppose the number density of molecules in the ground and excited states of **Figure 4** is n_0 and n_1, respectively. In view of the above description of the rate of change, the number density in the excited state by radiative and nonradiative transitions is given by

$$dn_1/dt = (r_{01} + c_{01})n_0 - (r_{10} + c_{10})n_1 = \rho(\nu)B_{01}n_0 - (\rho(\nu)B_{10} + A_{10} + c_{10})n_1$$
$$= \rho(\nu)B_{01}(n_0 - n_1) - (A_{10} + c_{10})n_1 \tag{2}$$
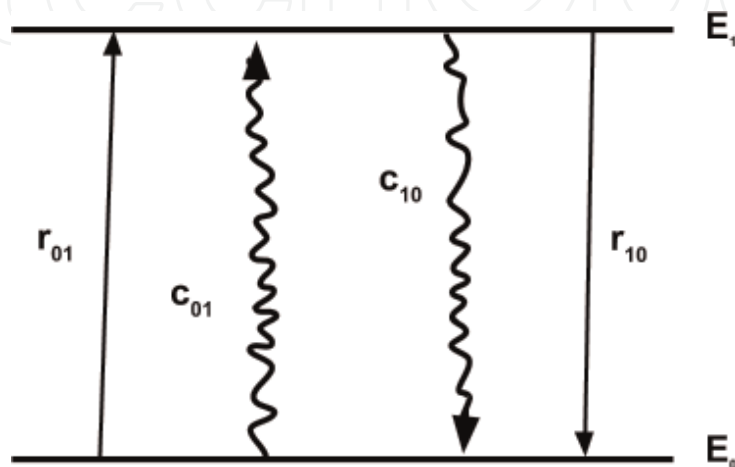
Figure 4.
Two-level molecular model showing the rate of radiative (r_{ij}) and nonradiative (c_{ij}) transitions between energy states E_0 and E_1.

We define the radiative and nonradiative lifetimes to be $\tau r = 1/A_{10}$ and $\tau c = 1/c_{10}$, respectively, and the total lifetime $\tau (1/\tau = 1/\tau r + 1/\tau c)$, to get the following expression for the rate of change of excited state population:

$$dn_1/dt = \rho(\nu)B_{01}(n_0 - n_1) - (1/\tau r + 1/\tau c)n_1$$
$$= \rho(\nu)B_{01}(n_0 - n_1) - n_1/\tau \tag{3}$$

In a similar manner, we find the following expression for the rate of change of ground state population density:

$$dn_0/dt = \rho(\nu)B_{01}(n_1 - n_0) + n_1/\tau \tag{4}$$

Hence from Eqs. (3) and (4), we get

$$dn_1/dt - dn_0/dt = 2\rho(\nu)B_{01}(n_0 - n_1) - 2n_1/\tau \tag{5}$$

In a photoacoustic experiment, we assume the incident light intensity I to vary slowly so that we may consider the upper and lower state population density changes to be an adiabatic interchange. Under this approximation we can set the left-hand side of Eq. (5) to zero. Since the total molecular density for the two-level system is $N = n_1 + n_0$, Eq. (5) takes the following form:

$$0 = 2\rho(\nu)B_{01}(n_0 - N + n_0) - 2(N - n_0)/\tau = 4\rho(\nu)B_{01}n_0 - 2N(\rho(\nu)B_{01} + 1/\tau) + 2n_0/\tau$$

Hence $\quad n_0 = N[\rho(\nu)B_{01} + 1/\tau]/(2\rho(\nu)B_{01} + 1/\tau)$

$$\tag{6}$$

$$\text{Similarly} \quad n_1 = N\rho(\nu)B_{01}/(2\rho(\nu)B_{01} + 1/\tau) \tag{7}$$

The spectral radiant energy density is directly proportional to the intensity I of the light source, and we define a constant $B = \rho(\nu)B_{01}/I$ so that Eq. (7) takes the following form:

$$n_1 = NBI/(2BI + 1/\tau) \tag{8}$$

Mechanical chopping of the light source at a frequency ω can be expressed as the periodic "on" and "off" of the intensity by $I = I_0 \cos\omega t$ for simplicity, and we get the following expression for the excited state population density:

$$n_1 = NBI_0\cos\omega t/(2BI_0\cos\omega t + 1/\tau) \tag{9}$$

If the gas is very weakly absorbing, we assume that most of the molecules are in state E_0 or $n_0 >> n_1$. Hence from Eqs. (6) and (7), $BI << 1/\tau$ so that Eq. (9) takes the following form:

$$n_1 = \tau NBI_0\cos\omega t \tag{10}$$

For a molecular gas, its kinetic energy (K) has to be considered to get the total internal energy density U of the two-level system leading to

$$U = n_1E_1 + K \tag{11}$$

The rate of change of energy is given by

$$dU/dt = (dn_1/dt)E_1 + dK/dt = [\rho(\nu)B_{01}(n_0 - n_1) - (A_{10} + c_{10})n_1]E_1 + dK/dt \tag{12}$$

This change of energy is equal to the difference between the absorbed and radiated optical energy so that

$$dU/dt = (r_{01}n_0 - r_{10}n_1)E_1$$
$$= [\rho(\nu)B_{01}(n_0 - n_1) - A_{10}n_1]E_1 \qquad (13)$$

We know that $A_{01} = 0$ and $c_{01} = 0$; hence from Eqs. (12) and (13), we get the following relation:

$$dK/dt = c_{10}n_1 E_1 \qquad (14)$$

Since the volume of the photoacoustic cell does not change in the experiment, and thermodynamic evaluation of the change in kinetic energy at constant volume gives

$$dK = (\delta K/\delta T)_V dT + (\delta K/\delta V)_T dV$$
$$= (\delta K/\delta T)_V dT \qquad (15)$$

Since the specific heat capacity of gas $C_V = (\delta K/\delta T)_V$, by integrating Eq. (15) we get

$$K = C_V T + f(V) \qquad (16)$$

where $f(V)$ is a constant of integration.

The pressure of the ideal gas $P = Nk_B T$, where N is the number density of molecules, k_B is the Boltzmann constant, and T is the temperature. Thus substituting for T from Eq. (16) in the expression for P, we get

$$P = Nk_B[K - f(V)]/C_V \qquad (17)$$

Since $f(V)$ is constant and the pressure wave (sound) is given by $\delta P/\delta t$, we get the following relation from Eq. (17) in the light of Eq. (14):

$$\delta P/\delta t = (Nk_B/C_V)dK/dt$$
$$= (Nk_B/C_V)c_{10}n_1 E_1 \qquad (18)$$

Substituting for n_1 from Eq. (10) and using the relation $c_{10} = 1/\tau c$, Eq. (18) reduces to

$$\delta P/\delta t = (k_B N^2 E_1/C_V)(\tau/\tau c)BI_0\cos\omega t \qquad (19)$$

Integrating Eq. (19) we get the following expression for photoacoustic signal, which is detected by a sensitive microphone:

$$P(t) = (k_B N^2 E_1/C_V)(\tau/\tau c)BI_0\sin\omega t \qquad (20)$$

2.2 Generation of photoacoustic signal in solids

Let us consider a cylindrical photoacoustic cell shown in **Figure 5** where the light-absorbing solid sample is surrounded by optically transparent gas (air) on the front side and the backing material is a poor conductor of heat. The absorption of light, of a particular wavelength in the sample, generates heat by nonradiative
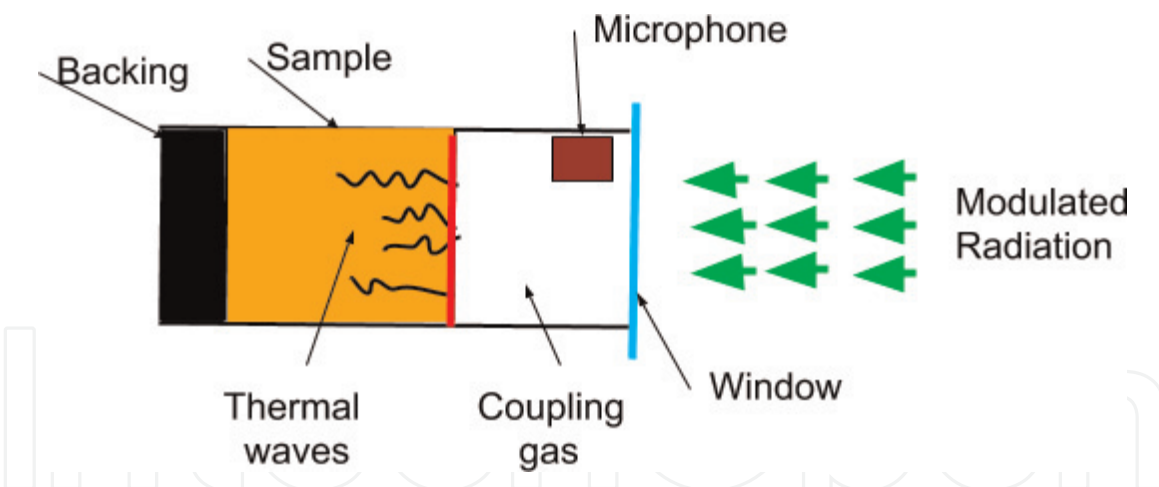
Figure 5.
Photoacoustic cell for a solid sample. Thermal waves originate from the point of absorption and travel toward the solid–gas interface to periodically heat a thin layer of gas (shown in red).

transitions. The acoustic signal produced in the coupling gas is due to periodic heat flow from the sample. Rosencwaig-Gersho model for PA signal generation depends on the optical as well as thermal properties of the solid sample [7]. The periodic heat flow from the solid sample heats a thin layer of coupling gas whose thickness depends on the frequency of chopping of the incident light (about 1 mm at 100 Hz). This layer (shown in red in **Figure 5**) may be imagined as a vibratory gas piston that creates the acoustic signal detected by the microphone. The intensity of light of wavelength λ transmitted through thickness "x" of the solid sample of absorption coefficient β is given by

$$I(\lambda) = I_0 \, e^{-\beta x} \tag{21}$$

where I_0 is the incident intensity for wavelength λ, and if ω is the modulation frequency of the incident radiation, the temporal variation of I_0 is given by

$$I_0(t) = (\tfrac{1}{2}) \, I_0 (1 + \cos\omega t) \tag{22}$$

The temperature variation in the gas dies out within a thickness of $2\pi\mu$ from the surface of the solid sample where μ is thermal diffusion length of the gas.

## 3. Experimental methods in photoacoustic spectroscopy (PAS)

The temperature and pressure changes involved in the process of PA signal generation are extremely small, typically a micro- to millidegree and nano- to microbar, respectively. This was the reason that the field of PAS remained dormant till the advent of tunable laser sources and of sensitive audio detectors. A piezo-electric transducer or a sensitive microphone serves as the acoustic detector in photoacoustic cells used during the laboratory experiments. Recent developments in the field of miniaturization and the related progress in computer software have made it possible to use tiny quartz-based acoustic detection devices like cantilever and crystal tuning forks. The photoacoustic spectrometer using miniature lasers fitted with these novel detectors can be easily packed in a small box and can be used in the laboratory or in the field for standoff detection of hazardous materials. The heat generated by the photoacoustic effect produces density changes caused by temperature fluctuations in liquid and gaseous samples. In such cases, photoacoustic spectroscopy is carried out by detection of thermal lens formation

using a probe laser. In the present case, however, we will confine to the detection of acoustic vibrations in the analysis of PA spectra.

## 3.1 Photoacoustic cells for gaseous samples

One of the simplest PA cells for measurements on gases and vapors is made from a Pyrex tube fitted with quartz windows at the two ends. The length of the tube and location of the microphone are chosen to maximize the PA signal using the resonance of sound generated by the modulated light beam. The design of such a cell made from 62.5-cm-long Pyrex tube of 2.5 cm diameter and fitted with quartz windows at Brewster's angle is shown in **Figure 6(a)**. The cell was resonant at 335 Hz with maximum signal in the middle port for the microphone, and it was resonant at 669 Hz, rendering maximum signal at two ports symmetrically located on either side of the middle port. The microphone ports correspond to the positions of three possible antinodes of the stationary acoustic waves formed at the two resonant frequencies. Acoustic isolation was achieved by putting the cell in a wooden box filled with sand. Two of the ports, not in use during the measurement, were sealed using O-rings and flat Teflon disks. PA measurements were carried out with iodine vapor at room temperature in the presence of air at atmospheric pressure using 20 milliwatt Argon laser light at 514.5 nm. The chopping frequency of the
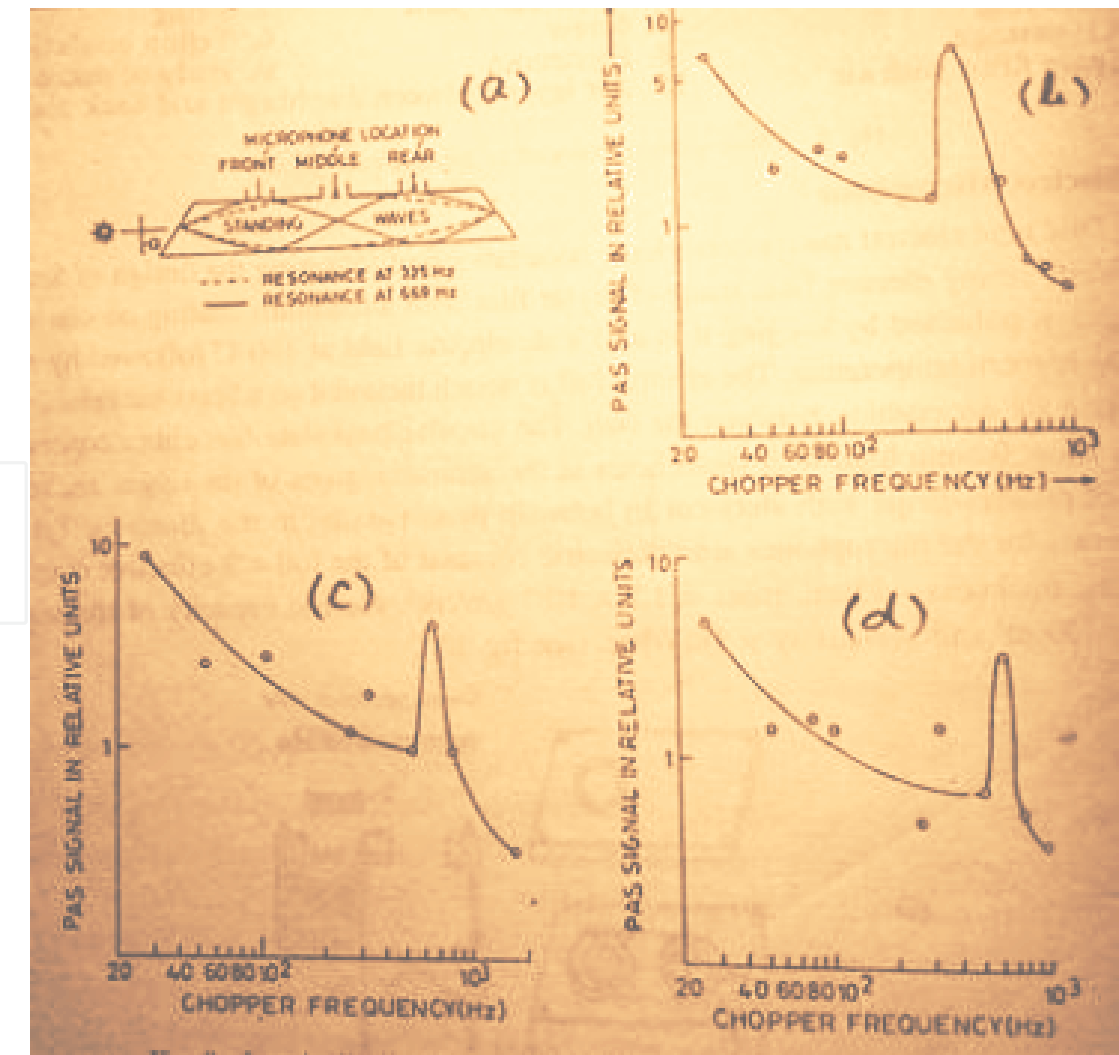
Figure 6.
Longitudinally resonant PA cell with three ports for microphone (a). PA signal for resonance at 335 Hz (b) and those for resonance at 669 Hz (c) and (d).

laser light was varied between 27 and 1000 Hz, and the resulting PA signals are shown in **Figure 6(b–d)** [8].

The photoacoustic spectrum of iodine vapor recorded using a Nd:YAG laser pumped tunable dye laser in the presence of atmospheric air and at 15 Torr is shown in **Figure 7**. Dye laser pulses used for the measurements were of 7 ns duration, 0.05 nm bandwidth, and 2mJ/pulse energy at a pulse repetition rate of 10 Hz. It is seen from the spectrum recorded with low air pressure in **Figure 7b** (upper half) that the relative intensity of vibronic bands monotonically increases in going up to the dissociation limit where I_2 molecule dissociates into a ground-state $(^2P_{3/2})$
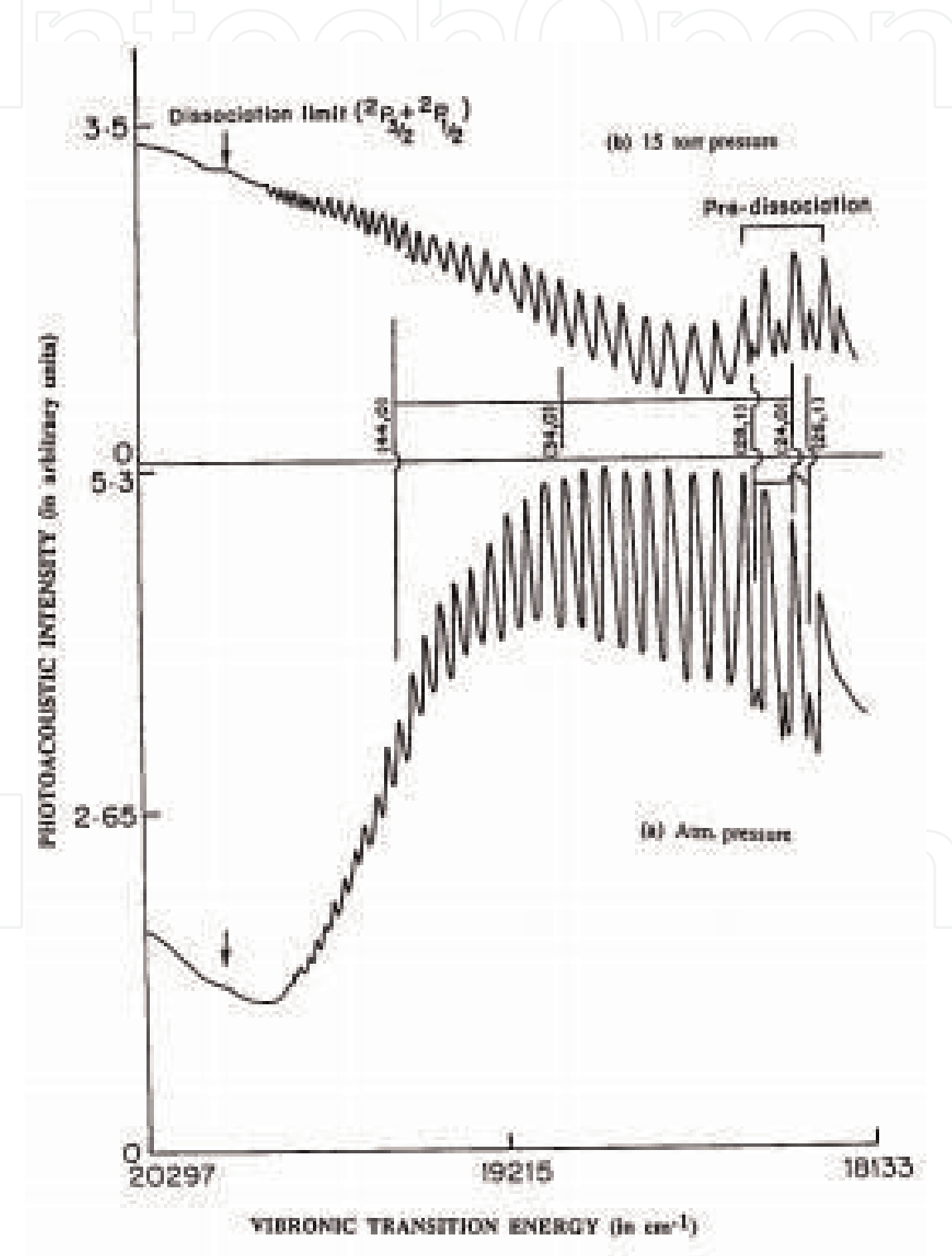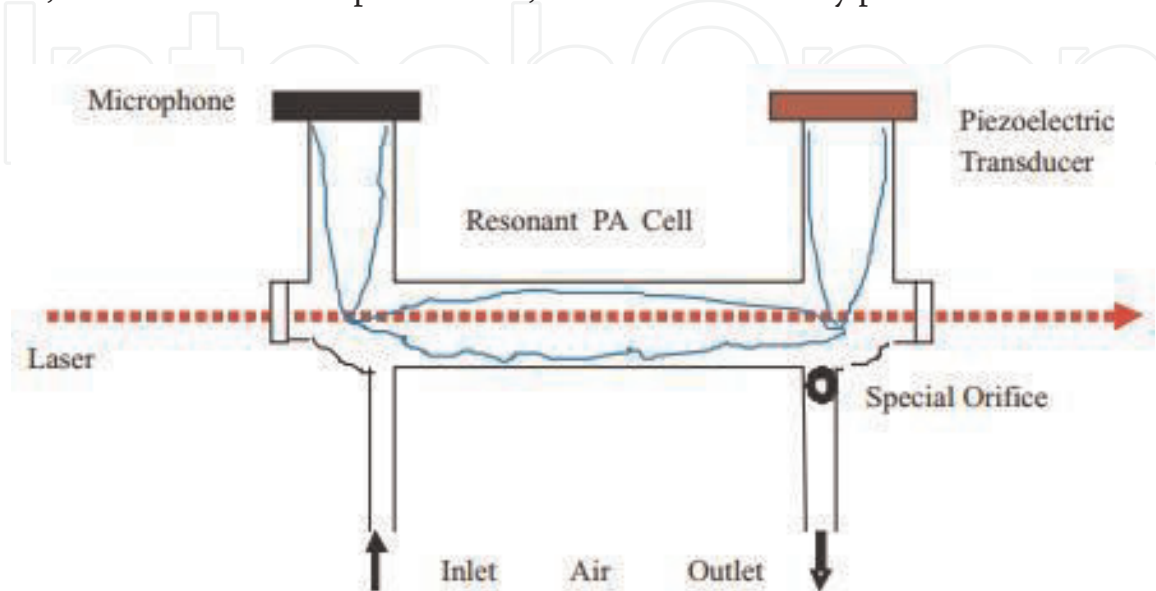

Figure 7.
Photoacoustic spectra of I_2 vapor in the wavelength region 492–552 nm (20,300–18,100 cm^{-1}). The little downward arrow indicates the wavelength of exciting radiation that dissociates I_2 into two iodine atoms (20,043 cm^{-1}).

iodine atom and an excited-state $\left(^2P_{1/2}\right)$ iodine atom. In **Figure 7a** for the spectrum recorded at atmospheric air, the relative intensity of vibronic bands monotonically decreases after maximum intensity at 19,225 cm^{-1} This reduction in intensity of the PA spectrum has been explained in terms of energy transfer from excited $\left(^2P_{1/2}\right)$ iodine atoms to O_2 molecules following the dissociation of I_2 [9].

To make photoacoustic measurements on a flowing gas sample, such as in the case of pollution monitoring, one needs a different type of acoustic resonant PA cell as schematically illustrated in **Figure 8**. The U-shaped cell has a total length L = λ, corresponding to the acoustic wavelength generated by the periodically modulated laser. The horizontal section of the tube is of length $\lambda/2$ and two vertical sections at each end of length $\lambda/4$. At the resonance frequency, a stationary wave is formed with antinodes at the two ends as well as at the center of the horizontal section and nodes at the two bent corners (see **Figure 8**). The laser as well as gas inlet and outlet, in the PA cell, is located near the nodes, which form regions of low pressure, of the stationary acoustic wave to prevent pressure fluctuations in PA signal at the antinodes. A microphone is fixed near the open end of one of the vertical arms, to detect the PA signal. A piezoelectric disk, fixed at the end of the other vertical arm, is used for detection of resonance frequency of the PA cell and the resonator quality factor to calibrate the system. There is a phase difference of 180° between high pressure points of the stationary acoustic wave at the center of the horizontal section, where heat is generated, and the two ends where microphone and piezo-electric signals are measured. The flow rate of the sample in the PA cell is controlled by a very narrow orifice at the outlet end, such that the pressure inside the PA cell remains steady. The special narrow hole causes a pressure drop of at least 50% on the outlet side compared to pressure inside the PA cell, while the airflow velocity through the orifice reaches the speed of sound. Since the air traveling through the orifice is moving out at the speed of sound, any sound from the pump traveling toward the PA cell, also at the same speed, meets a barrier in air, moving in the opposite direction, and it goes no further. This arrangement blocks the noise from the pump entering the PA cell and cluttering the PA signal.

The airborne particulate matter (aerosols) remains suspended in air inside the PA cell shown in **Figure 8** and has enough time to absorb radiation from the tunable laser beam. The absorbed optical energy is transferred as heat to the surrounding air, before the next laser pulse arrives, to build the stationary pressure wave in the
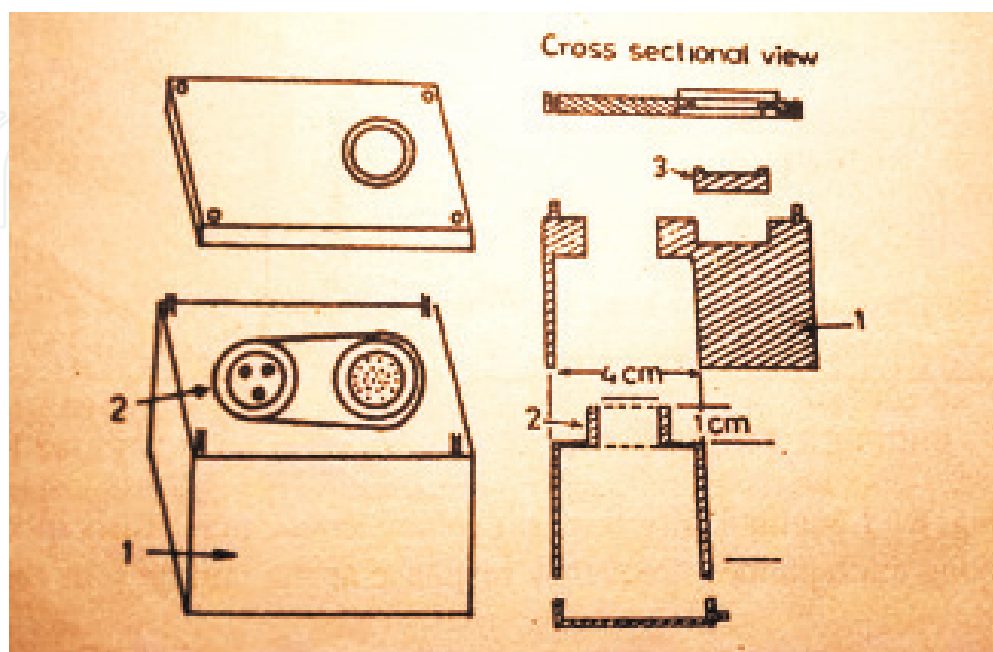

Figure 8.
The U-shaped resonant PA cell for detection of PA signal in a flowing air sample with special orifice for controlling the pressure inside the cell.

PA cell. An instrument of this type can directly measure light absorption by aerosols over the entire range of sunlight entering the atmosphere. This type of PA cell has been used with a single laser as well as with two lasers of different wavelengths impacting the same gaseous sample [10, 11].

3.2 Photoacoustic cells for solid samples

PA cells fitted with microphone, for recording PA spectra of solid samples, have been routinely used in the laboratory for almost four decades. One of the important aspects of homemade cells is to choose a material for effective shielding from extraneous sound. The design of a nonresonant PA cell is schematically shown in **Figure 9**. The main body of the cell has been constructed from a single block of aluminum with a cavity made from the bottom side for fixing the microphone along with its preamplifier. A cavity is made on the top of the block to put the sample cuvette whose open end is in the same horizontal plane as the microphone surface. A flat aluminum plate with double quartz windows in front of the sample cuvette is tightly fixed at the top of the main body with a very thin, suitably cut rubber sheet to make the chamber airtight. The thickness of the air duct connecting the sample and microphone is about 1 mm, and its total volume is less than 1 cc. The exterior dimensions of the stainless steel sample cuvettes are identical so as to tightly fit into their designated cavity. The sample cuvettes are, however, of varying depths to make measurements on powder samples of different thicknesses. Carbon black is used as the standard sample for recording the power spectrum of the excitation source of light to normalize the PA signals of the sample under investigation.

The PA spectra of powder samples of RDX and TNT recorded with a PA cell of the above type are shown in **Figure 10**. The source of excitation used in these experiments was a rotational line tunable cw CO_2 laser, and the window, in front of the sample in the PA cell, was made of flat ZnSe plate. The PA signals were measured manually from the lock-in amplifier and normalized using the power meter reading for each laser line. Microgram quantities of powder samples were used in the spectral measurements which exhibit the characteristic vibrational
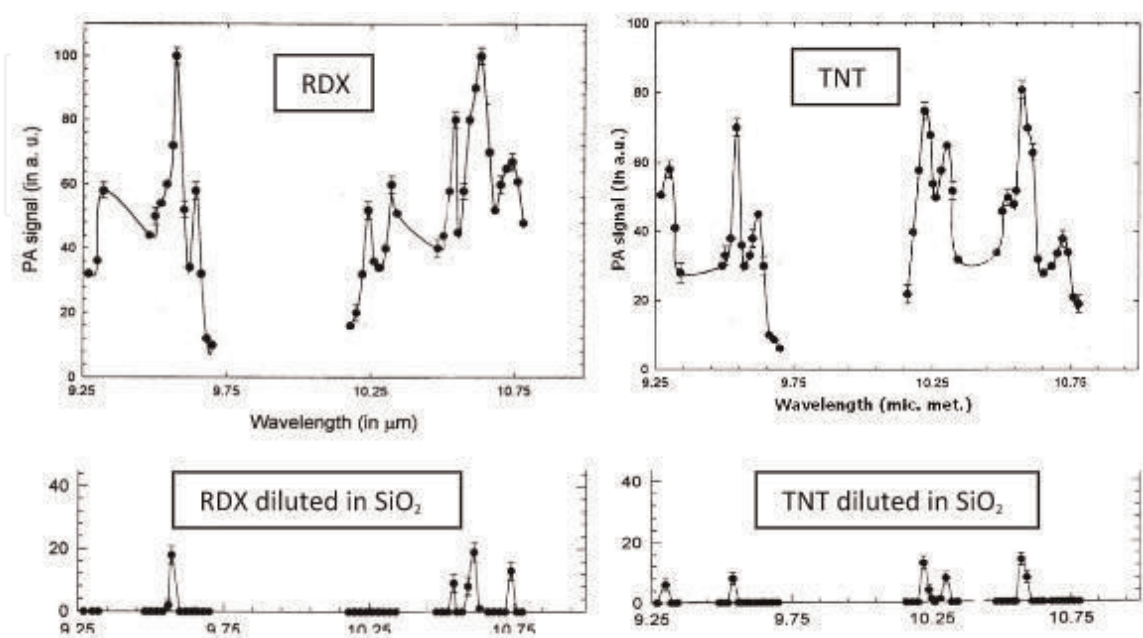

Figure 9.
Design of nonresonant PA cell. (1) the main body of aluminum, (2) microphone and preamplifier chamber, and (3) sample cuvette.

bands of RDX and TNT [12]. The solid circles in the upper half of **Figure 10** represent the normalized PA signals for the pure explosive powders in the rotational line tunable CO_2 laser wavelength range from 9.6 to 10.6 µm. The samples were diluted by uniformly mixing 10 micrograms of each explosive with 8 grams of SiO_2, which does not have any absorption in this region. Thus, the concentrations of the two explosives correspond to a few ppm, exhibiting four persistent bands of RDX and five of TNT with appreciable intensity as shown in the lower part of **Figure 10**.

3.3 PA spectroscopy of contaminated water

PA instrumentation for detection of liquid samples is somewhat complicated. A schematic diagram of the experimental setup for detection of harmful and dangerous pollutants in water is shown in **Figure 11**. The tunable dye laser beam, pumped by an excimer laser or a Nd:YAG laser, is focused into a 600 micron core multimode optical fiber for investigation on remotely located samples. The polluted water is kept in a quartz cuvette which is acoustically coupled to a piezoelectric transducer. The light exiting from the optical fiber is collimated into the quartz cuvette by means of a 10X microscope objective. The pulse to pulse energy fluctuation, in the light exiting from the cuvette, is monitored by a photodiode assembly, to ratio the PA spectra with the dye laser power profile. The PA signal and the photodiode signal are fed to two different gates of the boxcar, and the normalized spectrum is recorded by the computer by scanning the dye laser wavelength. The quartz cuvette with its piezoelectric transducer, the microscope objective, and the photodiode are fixed on a small portable platform which can be easily positioned within the glovebox for handling radioactive samples. Klenze et al. [13] have determined ultralow concentrations of Am^{3+} and Pu^{4+} in aqueous solutions with excimer laser-pumped dye laser, while Nd : YAG-pumped dye laser system was used by Russo et al. [14] to record PA spectra of aqueous solutions containing different concentrations of Pr^{3+} and Am^{3+}. Kim [15] has investigated the problem of actinide colloid generation in groundwater which plays a critical role in geochemical interaction and migration of actinides.

Figure 10.
CO_2 laser-excited PA spectra of RDX and TNT powders. The persistent vibrational bands of the two molecules are seen for highly diluted samples in the lower half of the figure.
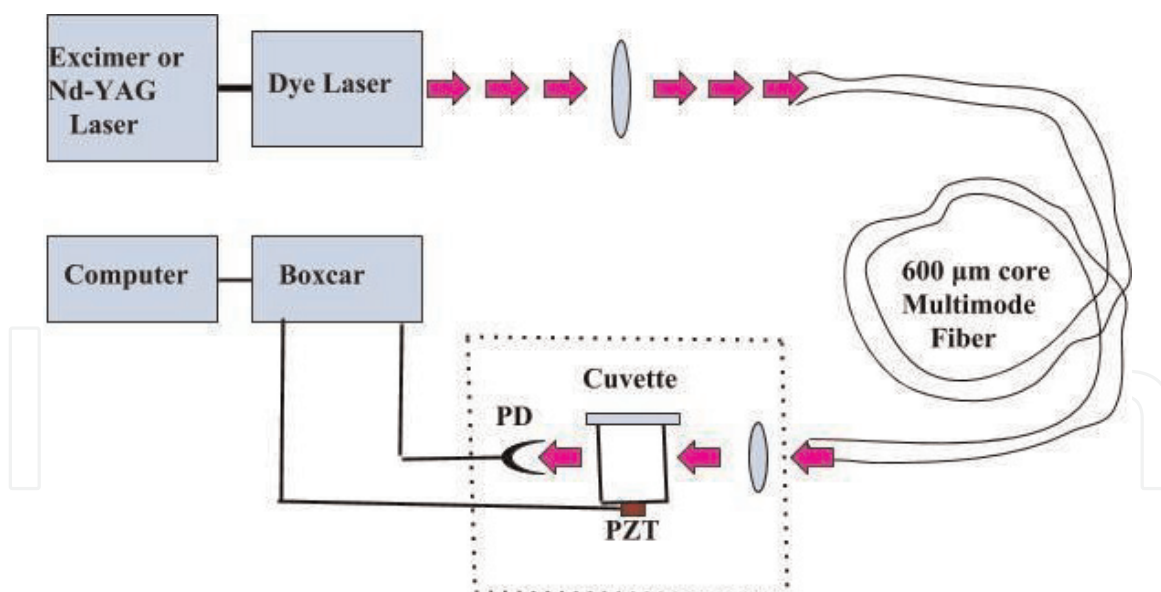
Figure 11.
Schematic PA spectroscopy system for trace detection of chemical species in polluted water.

3.4 Quartz tuning fork for PA detection

In a PA cell, the acoustic energy is accumulated in a resonant cavity, but the principle of PA detection by a quartz tuning fork (QTF) involves the accumulation of the acoustic energy in a sharply resonant acoustic transducer [16–18]. Crystal quartz is an easy material for such a transducer because of its low loss piezoelectric property, and QTFs can be designed to resonate at any frequency between 4 Hz and 200 kHz. The widely used QTF, manufactured for use in electronic clocks as frequency standard, resonates at 32,768 Hz in vacuum. The detection of PA signal by QTF is based on the piezoelectric effect produced by acoustic waves at the resonant frequency that mechanically bend its prongs. In the PA spectroscopy of gaseous sample, the interaction between the modulated laser beam and a trace gas generates acoustic waves that mechanically bend the QTF prongs. The voltage produced by the piezoelectricity generates the PA signal.

When a laser beam is focused at the center between the two prongs of the QTF placed in a gaseous sample, the absorbed optical energy converted into heat generates a weak acoustic pressure wave. When the laser beam is modulated at half the QTF resonant frequency (f), the pressure wave makes the two prongs move apart two times during each acoustic cycle. In this situation the QTF detects sound oscillations at the second harmonic of the modulation frequency due to two absorption events during each modulation period. The laser light is modulated at "f/2" and PA signal demodulated by lock-in amplifier at "f" as shown in **Figure 12**. The PA spectrum is recorded by varying the wavelength of the tunable laser.

The use of QTF for solid phase PA detection in the laboratory requires a very thin film of the molecular sample to be adsorbed on the outer surface of one of the prongs. The absorbed laser light heats the sample, generating an acoustic wave at the prong's surface interface with air. When the frequency of repetition of the incident laser pulse coincides with the mechanical resonant frequency of the QTF, the localized pressure variation sets the latter into vibration. The amplitude of this vibration and the resulting piezoelectric voltage are proportional to the amount of heat produced by optical absorption at the surface.

An experimental arrangement using the above concept is schematically shown in **Figure 13** using a quantum cascade laser (QCL). The large wavelength coverage in
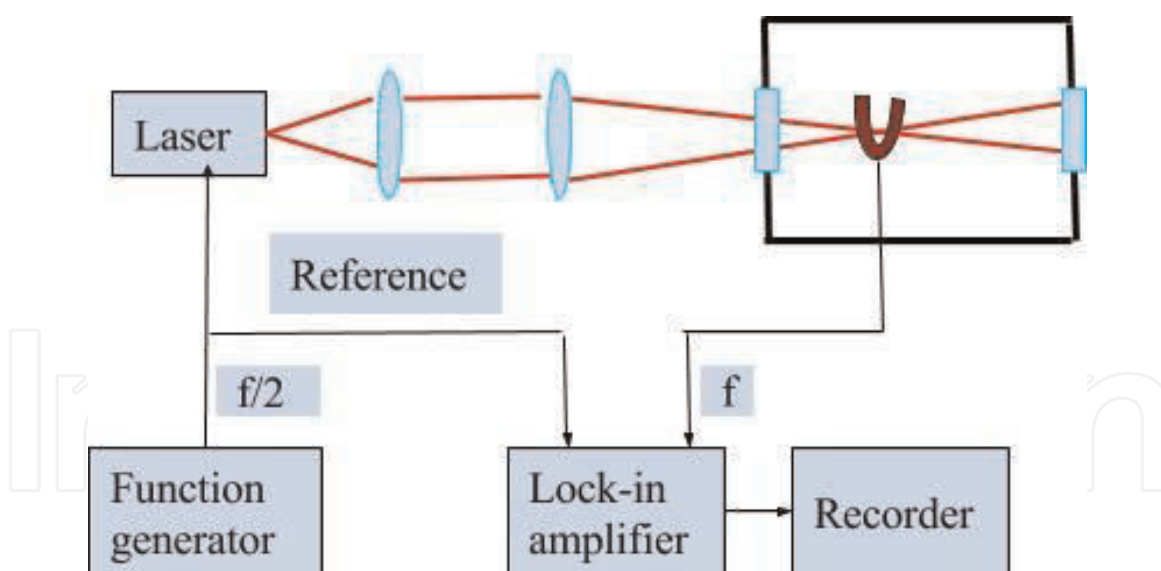
Figure 12.
Experimental setup for gas phase PA spectroscopy with QTF detector. The excitation diode laser source is currently modulated at half of the QTF resonant frequency (f).
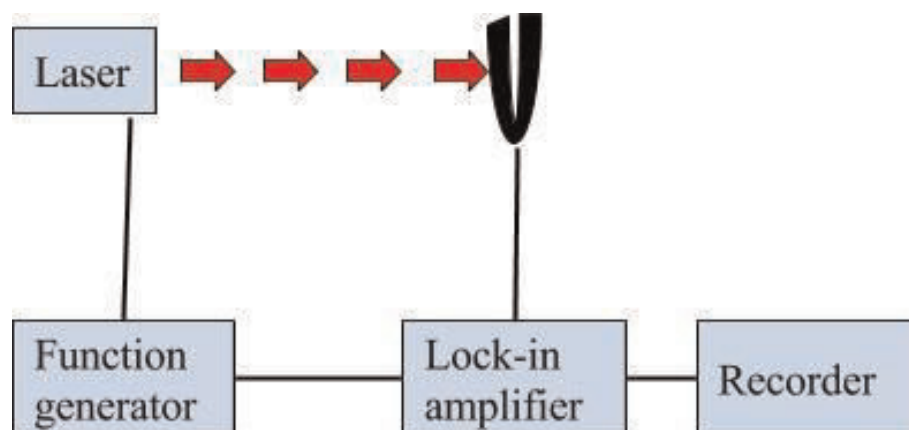
Figure 13.
Schematic experimental arrangement for solid phase PA spectroscopy using QTF detector with sample adsorbed on one of the QTF prongs. The function generator controls the pulse repetition rate of the quantum cascade laser (QCL) to be in resonance with the symmetric vibration of the QTF.

the mid-IR region combined with narrow linewidth and powering up to tens of mW of QCL proves ideal for trace detection of molecules [19]. This system can be employed in trace detection of several molecular species adsorbed on the surface of the prong. A variant of this system has been used in detection of adsorbed chemicals on surfaces remotely located from the laser [20].

4. Photoacoustic detection of harmful chemicals

PA spectroscopy has been widely used in chemical sensing applications in environmental science and medical diagnostics. It is useful in rapid detection of illicit drugs, nerve agents, and hazardous biological materials. In a typical hospital environment, there is a need for evaluation of anesthetic gaseous components. Although hospital staff are exposed to much lower anesthetic concentration than the patients, this exposure extends over many years. Under inadequate hygiene conditions, people working in hospitals or factories often complain of headaches and fatigue due to traces of harmful gases in the environment. Illicit drug trafficking poses many challenges for detection of dangerous chemicals that threaten life and

property. In the following sections, we will present examples of point detection as well as standoff detection of chemical compounds using PA spectroscopy.

4.1 PA spectroscopy of ethylene

Ethylene (C_2H_4) is a well-known emission fingerprint from vehicle exhausts and its reaction with nitric oxides under solar UV radiation produces ozone. Altuzar et al. [21] have used a CO_2 laser with PA cell located inside the laser cavity to profit from the intracavity laser power. A mechanical chopper modulated the intensity of the laser beam at a frequency that matches with the acoustic resonant frequency of the PA cell. The 10P14 line of CO_2 laser is in exact resonance with the Q branch of the ν_7 band of ethylene. Air samples from different locations in Mexico city were collected from 6 to 9 am in the morning and from 12 to 15 pm in the afternoon. The raw samples, collected in stainless steel vessels, went through the process of removing CO_2 and water vapor before being transferred into the PA cell. The results of ethylene concentration analysis exhibit higher values in samples collected in the morning and lower values for the afternoon samples. The increased concentration of ethylene is attributed to emission from vehicles when the morning traffic is heavy. The decrease of ethylene concentration in the afternoon samples has two possible causes. Firstly, there is expansion in the thickness of atmospheric air, due to heating by sunlight leading to dilution of ethylene. Secondly, ethylene reacts with nitrogen oxides in the presence of solar UV radiation to produce ozone and other oxidants, causing a decrease in its concentration. It is to be emphasized that PA technique has the advantage of performing online measurements with excellent time resolution.

## 4.2 PA spectroscopy of gases emanating from the human body

The smells emanating from various parts of the body are unique to an individual, made up of specific chemical compounds that vary depending on age, diet, metabolism, and health. Near-IR diode laser at $1.53\,\mu m$ has been used in PA detection of ammonia concentrations in ppmV and ppbV range by several workers [18, 22]. Although NH_3 is biosynthesized through normal amino acid metabolism, it is toxic in high concentrations, and its amount in blood gets elevated due to liver dysfunction. Compact quantum cascade lasers (QCL) may prove to be an important mid-IR source for portable ammonia sensors.

Trace level detection of nitric oxide has many applications in medicine, biology, and environmental science. CO laser was the first to be used by Kreuzer and Patel [2] for PA detection of NO concentrations of 0.01 ppmV. Since its first detection in exhaled air [23], NO has been found to be a sensitive marker for asthmatic airway inflammation [24]. A QCL-based PA cell has been developed by Elia et al. [25], while Spagnolo et al. have reported a minimum NO concentration limit of 15 ppbV [26].

A CO_2 laser has been used as the source of PA excitation by Harren et al. [27] to detect the emission of ethylene from the human breath and skin under exposure to UV radiation. In this experiment a small amount of exhaled air was cleaned for its content of CO_2, water vapor, and other spectroscopically interfering gases, before introducing it into the PA cell. The 10P14 emission line of CO_2 laser was used to detect a lower limit of 6 ppbV ethylene in nitrogen.

4.3 PA spectroscopy of dangerous drugs

Morphine is the prototype narcotic drug, and it is the standard against which all other opioids are tested. An acetylated form of morphine, almost two times more
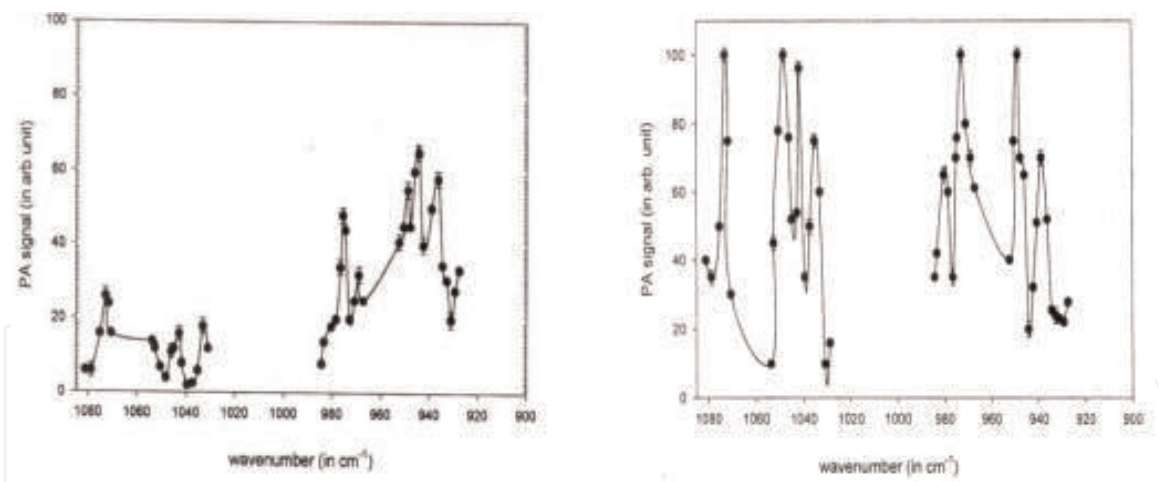
Figure 14.
CO$_2$ laser-excited PA spectra of powders of heroin (on the left) and morphine (on right).

potent than morphine itself, is known as heroin. Animal and human studies and clinical experience back up the contention that morphine is one of the most euphoric drugs on earth. Both morphine and heroin are used for pain medication, but both are addictive and identified as illegal drugs.

Microgram quantities of powders of morphine and heroin were used in a PA cell shown in **Figure 9** and fitted with ZnSe window. Rotational line tunable CO$_2$ laser was used as the excitation source for recording the PA spectra of the two compounds shown in **Figure 14**. The black dots in the figures represent the manually measured PA signals from the lock-in amplifier normalized by laser power at each wavelength. The spectral peaks correspond to the vibrational bands of morphine and heroin in the wavelength range 9.6 to 10.6 micron [28].
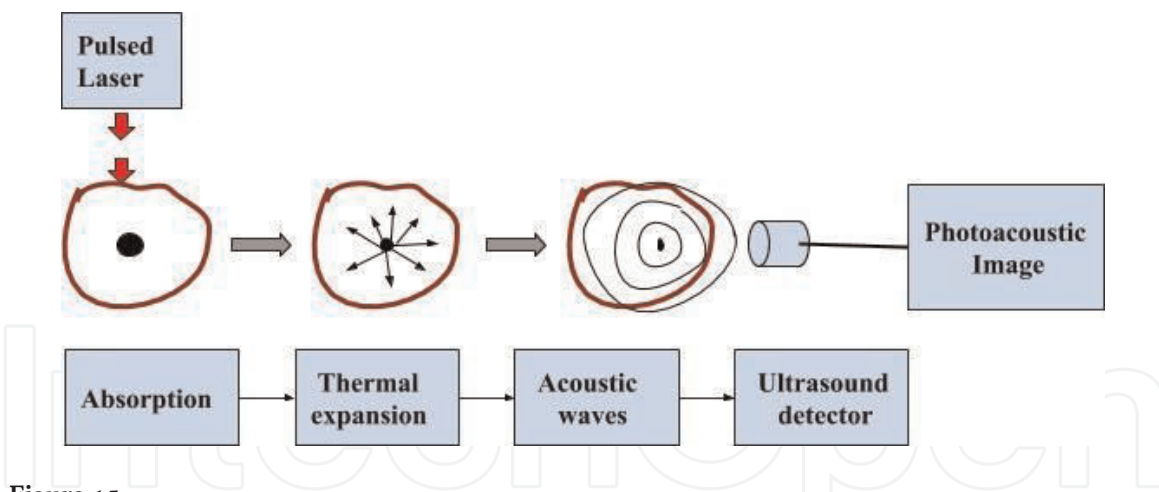
5. Photoacoustic imaging

Photoacoustic imaging is an emerging technique that combines the high resolution of light and deep imaging capability of ultrasound. It is similar to hyperspectral imaging except for the fact that optical sensors are replaced by ultrasonic detectors that convert the sound waves into images. It has many applications as a noninvasive technique in medicine to produce molecular images of internal organs. It is based on the rapid production of heat, when the optical energy from a nanosecond laser pulse is absorbed in the tissue, causing thermal expansion and the generation of ultrasonic waves. The processes involved in the image formation are schematically illustrated in **Figure 15**, which show that it is a hybrid technique making use of optical absorption and ultrasonic wave propagation.

There are two basic conditions for efficient generation of the PA signal for imaging. The condition of "thermal confinement" requires the laser pulse duration τ_p to be shorter than temporal duration τ_{th} of thermal diffusion from the heated volume. This condition implies that there is negligible heat diffusion during the laser pulse so that the PA image essentially reveals the initial absorbed energy distribution in the sample. The second condition of "stress confinement" requires that time τ_s for stress to transit the heated volume should be longer than the laser pulse duration τ_p.

It can be shown that a nanosecond laser pulse impacting a biological tissue sample satisfies the conditions for PA imaging. Thermal diffusion length during the laser pulse is given by $\delta_T = 2(\tau_p D_T)^{1/2}$ where D_T is the thermal diffusivity of the

16

Figure 15.
Schematic illustration of the principle and processes involved in photoacoustic image formation.

sample. A typical value of $D_T = 1.4 \times 10^{-3} \text{cm}^2/\text{s}$ for most tissue [29] gives $\delta_T = 0.05 \mu\text{m}$ for a laser pulse of $\tau_p = 5$ ns. Duration of thermal diffusion is given by $\tau_{th} = L^2/4D_T$ where L is the radius of the spherical shell of heat propagation in the sample. Thus for $L = 15 \mu\text{m}$, we get $\tau_{th} = 0.4$ ms. If "v" is the velocity of sound in tissue, the time taken by the stress to transit a sample length L in the heated region is given by $\tau_s = L/v$. Assuming $v = 1.5 \text{mm}/\mu\text{s}$ we get $\tau_s = 10$ ns. This simple calculation shows that we would achieve a spatial resolution of $15 \mu\text{m}$ in the PA image if $\tau_s = 10$ ns and $\tau_{th} = 0.4$ ms. Thus we find that the process of heat generation by a 5 ns laser pulse would satisfy the two conditions for generating PA signals efficiently.

5.1 Photoacoustic microscopy and photoacoustic tomography

Photoacoustic tomography (PAT) and photoacoustic microscopy (PAM) are the two methods of PA imaging. In the PAT mode, an expanded laser beam illuminates the whole sample, and laser photons are absorbed at various points in the sample generating ultrasonic waves. PAT acquires depth-dependent information by time-of-flight measurements of the acoustic waves. An ultrasonic transducer placed outside the sample detects the PA signal, which is measured either by moving a single transducer around the sample or by using an array of transducers. PA image is obtained from the data set of PA signals by using appropriate reconstruction algorithms in the computer. In the case of PAM, the laser beam is focused into a tiny volume, and ultrasonic waves from this localized region are imaged by the detector. To obtain a 3D image, transverse sections at different depths in the sample are scanned in two dimensions. The axial resolution of the image can be as good as the optical resolution ($< 1 \mu\text{m}$) where the depth information is determined by the time of flight of ultrasonic waves.

5.2 Photoacoustic microscopy of zebra fish

Fluorescence microscopy is an effective tool in thin biological samples like single-celled organisms, but with slightly thicker samples, it becomes difficult to know where exactly the fluorescence originates. In a complex organism, like zebra fish, it is crucial to image deeper and deeper while the organism is kept alive. Fluorescent light emerging from the point of absorption suffers multiple scattering in the tissue on its way to the optical detector. This leads to loss of information on the origin and propagation path of the fluorescent light, giving rise to a blurred

image and destruction of the spatial resolution. PA detection of optical absorption circumvents these limitations, because the sound waves travel through the diffuse biological media with much less distortion than light.

The experimental components used in PAM by Harrison et al. [30] are shown in **Figure 16a**. The laser beam, from a tunable source (L), is diverted down the 45° reflecting cone R, by the prism P. The curved surface of the cone directs the laser beam in a horizontal plane which is reflected downward by the corner polished surfaces inclined at 45° with the horizontal plane. The laser beam then travels downward along the longer sides of the ultrasound probe (T) to be focused about 10.5 mm below the bottom of the probe (see **Figure 16a**). The position of the ultrasound transducer (T) is adjusted vertically to match its focus with the laser focus by maximizing the PA signal from carbon fiber sample [30]. The combined ultrasound and laser light probe is mounted on a voice coil (VC) stage which is driven by a programmed motor controller to achieve oscillations at 10 Hz over a length of about 10 mm. The imaging system can be run in three different modes, (i) ultrasound mode, (ii) PA mode, and (iii) interlaced PA-ultrasound mode, and it can produce images of microvascular structures to depths of 2–3 mm in vivo as illustrated in **Figure 16b** for zebra fish.

In the recording of images of **Figure 16b**, the zebra fish was held on a rotating platform immersed in water. The position of the laser focus was fixed at a particular depth inside the body of the sample, and the platform was rotated through 360° to record the two-dimensional sections [31]. The location of fluorescent protein mCherry (in red) is clearly seen in the image of the zebra fish brain at the top, and transverse image slices of the zebra fish hindbrain are shown in the lower half of **Figure 16b**, where each slice is separated by a depth of 0.5 mm inside the tissue.

5.3 Photoacoustic imaging of prostate cancer

PA imaging is emerging as a new diagnosis technique with specificity, high resolution, and enough imaging depth for early detection of prostate cancer. Ex vivo multispectral PA imaging has been carried out to differentiate between malignant
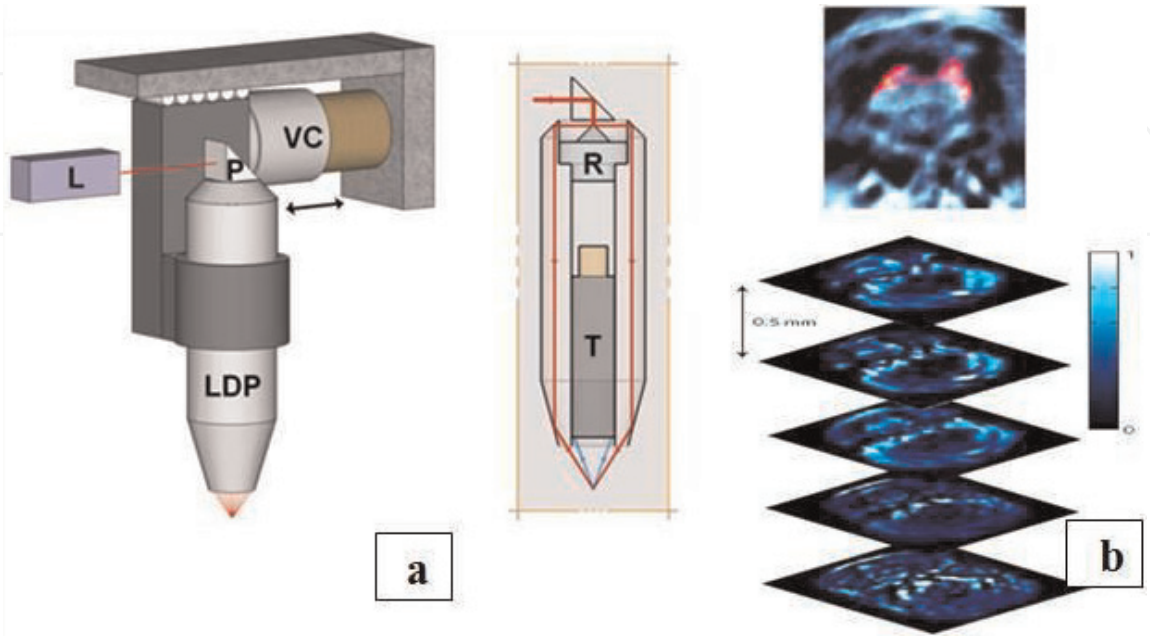
Figure 16.
(a) Experimental setup for combined photoacoustic (PA) and ultrasound (US) imaging (with permission from Ref. [30]). (b) In vivo image of a section of the zebra fish brain and five transverse image slices through the hindbrain (with permission from Ref. [31]).

prostate tissue, benign prostatic hyperplasia (BPH), and normal human prostate tissue. The preliminary results of investigations carried out by Dogra et al. [32] show that there was a significant difference in the mean PA intensity of dehydroxy hemoglobin (dHb) and lipid between malignant and normal prostate. There was also a significant difference in the mean intensity of dHb between malignant prostate and BPH. There was, however, no significant difference in HbO2, dHb, and lipid between normal prostate tissue and BPH. Laser radiation at 1064 nm and 1197 nm has been used to obtain PAT images, corresponding to optical absorption of hemoglobin and lipid, to determine the clustering prostate cancer tissue at each wavelength [33]. It was found that 1064 nm PAT in conjunction with ultrasound image is more effective in identifying prostate cancer biopsy targets than the PAT at 1197 nm.

6. Conclusion

This chapter starts with a brief history of photoacoustic effect and photoacoustic spectroscopy. A simple mathematical derivation for the generation of PA signal in gaseous and solid samples is followed by experimental methods. The design and construction of a variety of PA cells and detectors have been described along with their use in the investigation of gaseous, solid, and liquid samples. Some illustrative examples of trace detection of explosives and harmful chemicals have been discussed. A brief account of the principle and application of the emerging technique of PA imaging is discussed at the end of the chapter.

Acknowledgements

Author details

Surya Narayan Thakur
Banaras Hindu University, Varanasi, India

*Address all correspondence to: snthakur@gmail.com

IntechOpen

References

[1] Bell AG. On the production and reproduction of sound by light. American Association for the Advancement of Science. 1880;**29**:115

[2] Kreuzer LB, Patel CKN. Nitric oxide air pollution: Detection by optoacoustic spectroscopy. Science. 1971;**173**:45

[3] Tyndall JG. Action of an intermittent beam of radiant heat upon gaseous matter. Royal Society of London. 1881;**31**:307

[4] Bell AG. Upon the production of sound by radiant energy. Philosophical Magazine. 1881;**11**:510

[5] Kasha M. Characterization of electronic transitions in complex molecules. Discussions of the Faraday Society. 1950;**9**:14

[6] Lewis GN, Kasha M. Phosphorescence and the triplet state. Journal of the American Chemical Society. 1944;**66**:2100

[7] Rosencwaig A, Gersho A. Theory of the photoacoustic effect with solids. Journal of Applied Physics. 1976;**47**:64

[8] Thakur SN. Photoacoustic spectroscopy of gases and powders. Bulletin of Laser and Spectroscopy Society of India. 1993;**7**:3

[9] Narayanan K, Thakur SN. Photoacoustic spectrum of iodine in the 490–680 nm (20402–14700 cm^{-1}) region. Applied Optics. 1992;**31**:4987

[10] Arnott WP, Moosmuller H, Rogers CF, Jin T, Bruch R. Photoacoustic spectrometer for measuring light absorption by aerosol: Instrument description. Atmospheric Environment. 1999;**33**:2845

[11] Lewis KA, Arnott WP, Moosmuller H, Wold CE. Strong spectral variation of biomass smoke light absorption and single scattering albedo observed with a novel dual-wavelength photoacoustic instrument. Journal of Geophysical Research. 2008;**113**:D16203

[12] Prasad RL, Prasad R, Bhar GC, Thakur SN. Photoacoustic spectra and modes of vibration of TNT and RDX at CO_2 laser wavelengths. Spectrochimica Acta. 2002;**A58**:3093

[13] Klenze R, Stumpe R, Kim JI. Laser-induced photoacoustic spectroscopy for the speciation of actinides in submicromol concentrations. In: Hess P, Pelzl J, editors. Photoacoustic and Photothermal Phenomena. Heidelberg: Springer-Verlag; 1988. p. 139

[14] Russo RE, Rojas D, Robouch PB, Silva RJ. Remote photoacoustic measurements in aqueous solutions using an optical fiber. The Review of Scientific Instruments. 1990;**61**:3729

[15] Kim JI. Actinide colloid generation in groundwater. Radiochimica Acta. 1991;**52/53**:71

[16] Kosterev AA, Bakhirikin YA, Curl RF, Tittle FK. Quartz-enhanced photoacoustic spectroscopy. Optics Letters. 2002;**27**:1902

[17] Weidmann D, Kosterev AA, Tittle FK, Ryan N, McDonald D. Application of widely electrically tunable diode laser to chemical gas sensing with quartzenhanced photoacoustic spectroscopy. Optics Letters. 2004;**29**:1837

[18] Kosterev AA, Tittle FK. Ammonia detection using quartz-enhanced photoacoustic spectroscopy with a near-IR telecommunication diode laser. Applied Optics. 2004;**43**:6213

[19] Kosterev AA, Tittle FK. Chemical sensors based on quantum cascade

lasers. Journal of Quantum Electronics. 2002;**38**:582

[20] Van Neste CW, Senesac LR, Thundat T. Standoff photoacoustic spectroscopy. Applied Physics Letters. 2008;**92**:234102

[21] Altuzar V, Pacheco M, Tomás SA, Arriaga JL, Zelaya-Angel O, Sánchez-Sinencio F. Analysis of ethylene concentration in the Mexico City atmosphere by photoacoustic spectroscopy. Analytical Sciences (Special Issue) The Japan Society for Analytical Chemistry. 2001;**17**:s541

[22] Schmohl A, Miklos A, Hess P. Detection of ammonia by photoacoustic spectroscopy with semiconductor lasers. Applied Optics. 2002;**41**:1815

[23] Gustafsson LE, Leone AM, Persson MG, Wikuld NP, Moncada S. Endogenous nitric oxide is present in the exhaled air of rabbits, guinea pigs and humans. Biochemical and Biophysical Research Communications. 1991;**181**:852

[24] Lanz MJ, Leung DYM, McCormick DR, Harbeck R, Szefler SJ, White CW. Comparison of exhaled nitric oxide, serum eosinophilic cationic protein, and soluble interleukin-2 receptor in exacerbations of pediatric asthma. Pediatric Pulmonology. 1997;**24**:305

[25] Elia A, Lugara PM, Giancaspro C. Photoacoustic detection of nitric oxide by use of a quantum-cascade laser. Optics Letters. 2005;**30**:988

[26] Spagnolo V, Kosterev AA, Dong L, Lewicki R, Tittle FK. NO trace gas sensor based on quartz-enhanced photoacoustic spectroscopy and external cavity quantum cascade laser. Applied Physics. 2010;**B100**:125

[27] Harren FJM, Gotti G, Oomens J, Hekkert St L. Photoacoustic spectroscopy in trace gas monitoring. In: Meyers RA, editor. Encyclopedia of Analytical Chemistry. Chichester: John Wiley; 2000. pp. 2203-2226

[28] Prasad RL, Thakur SN, Bhar GC. CO_2 laser photoacoustic spectra and vibrational modes of heroin, morphine and narcotine. Pramana. 2002;**59**:487

[29] Duck FA. Physical Properties of Tissue: A Comprehensive Reference Book. London: Academic Press; 1990

[30] Harrison T, Ranasinghesagara JC, Lu H, Mathewson K, Walsh A, Zemp R. Combined photoacoustic and ultrasound biomicroscopy. Optics Express. 2009;**17**(412)

[31] Razansky D, Distel M, Vinegoni C, Ma R, Perrimon N, Koster RW, et al. Multispectral opto-acoustic tomography of deep-seated fluorescent proteins in vivo. Nature Photonics. 2009;**3**:412

[32] Dogra VS, Chinni BK, Valluru KS, Joseph JV, Ghazi A, Yao JL, et al. Multispectral photoacoustic imaging of prostate cancer: Preliminary ex-vivo results. Journal of Clinical Imaging Science. 2013;**3**:41

[33] Bungart BL, Lan L, Wang P, Li R, Koch MO, Cheng L, et al. Photoacoustic tomography of intact human prostates and vascular texture analysis identify prostate cancer biopsy targets. Photoacoustics. 2018;**11**:48